Modeling of the ATRcoP Processes of Methyl Methacrylate and 2-(Trimethylsilyl) Ethyl Methacrylate in Continuous Reactors: From CSTR to PFR

Wei Wang, Yin-Ning Zhou, Zheng-Hong Luo*

From the chemical reactor engineering viewpoint, the material flow pattern in continuous reactor can influence the reaction characteristics and reactor performance. Based on the molar balance equations and the method of moments, a tubular reactor model was developed, which was validated using the experimental data from the open reports. Then the atom transfer radical copolymerization (ATRcoP) of methyl methacrylate (MMA) and 2-(trimethylsilyl) ethyl methacrylate (HEMA-TMS) under different axial dispersions in tubular reactors were simulated using the developed model. The main ATRcoP behaviors and polymer micro-characteristics were obtained. Finally, the effects of flow patterns (including the CSTR and PFR modes) on the ATRcoP characteristics were investigated using the models. The simulation results show that the reaction characteristics of the same ATRcoP system produced in flow with different axial dispersion levels are obviously different. Moreover, the comparison of properties such as monomer conversion, dispersity, copolymer composition, and chain-end functionality between two extreme flow patterns, i.e plug flow in tubular reactor and completely mixed flow in CSTR, were performed. The compositions along the copolymer chain for the two flow modes are very close. As for the other three properties, the tubular reactor has its own comparative advantages over the CSTR.

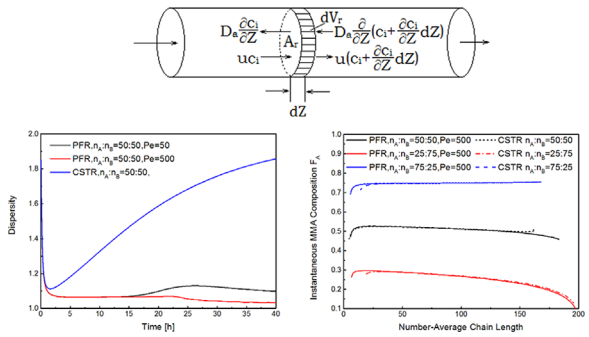

1. Introduction

Atom transfer radical (co) polymerization (ATR(co)P) has been demonstrated to be one of the important reversible-deactivation radical polymerization (RDRP) technologies for preparing (co) polymers with complex architectures in a controlled manner.[1] However, to increase commercial viability, ATPcoP could be combined with a continuous and variable process that is popular in industry.[2] From a chemical engineering standpoint, the material flow pattern in continuous reactor is complicated and it has important impact on reaction characteristics.[3] In general, two ideal flow patterns, i.e., complete mixing flow and plug flow modes, were involved in literature.[4–6] The actual material flow in continuous reactors is somewhere between the two ideal flow patterns. Furthermore, in a large-scale chemical process, there are always differences in the performance of a certain

W. Wang, Y.-N. Zhou, Prof. Z.-H. Luo
Department of Chemical Engineering, School of Chemistry and Chemical Engineering, Shanghai Jiao Tong University, Shanghai 200240,, P. R. China
E-mail: Luozh@sjtu.edu.cn
Fax: +86 21 54745602

Macromol. React. Eng. **2015,** DOI: 10.1002/mren.201400056

reaction system in different flow patterns. For such RDRP systems like ATRP, the life time of living chains is much longer than that for traditional free radical polymerization, and the concentration distribution of living chains can be greatly influenced by flow pattern of reactants during the polymerization. Therefore, the properties of polymeric products will also be significantly affected. Accordingly, combining continuous ATRP with industrial flow pattern would introduce many research topics. Among them, the basic research work, such as the flow pattern division, the flow pattern effect and mechanism etc.[2,7] The study of the transition and its effect of these two ideal flow patterns is helpful for the understanding of ATRcoP process in continuous reactors and the next industrial scale-up.

To date, most of the work with continuous RDRPs have been done in laboratory-scale systems.[8–25] Zhang and Ray[8] simulated the reversible addition fragmentation termination (RAFT) polymerization of methyl methacrylate (MMA) in a single CSTR and a series of CSTRs. Chan et al.[5,9,10] studied the ATRP under non-ideal mixing flow condition in a laboratory-scale CSTR. They also performed a continuous ATRP with low catalyst concentration in a tubular reactor.[11] Schork et al. studied the mini-emulsion RAFT polymerization in a train of CSTRs[12–14] and a multi-tube/tubular reactor,[15–17] respectively. Shen et al.[18–20] successfully developed a continuous column reactor packed with silica gel for continuous ATRP of MMA. Recently, an overview of copper-mediated controlled radical polymerization in continuous flow processes has been reported.[21] More recently, the ATRcoP of MMA and 2-(trimethylsilyl) ethyl methacrylate (HEMA-TMS) under the CSTR pattern were simulated in our group.[22,23] In summary, the polymerization behaviors of continuous RDRPs in two types of reactors (CSTR and tube reactor) are described based on varying polymer systems. Although two ideal flow modes have been applied in continuous ATRP systems separately, no systematic study that assesses their copolymerization kinetics within the same system has been conducted. Moreover, to the best of our knowledge, thus far there is no open report regarding the transition of these two ideal flow patterns within the same continuous ATRcoP system.

As described above, continuous RDRPs have been performed in tubular reactor and the effect of backmixing has also been observed in the previous works.[15–20,25] Unfortunately, the true flow effects in tubular reactor were generally ignored, which can be reflected via these non-ideal factors like molecule diffusion, vortex flow and velocity distribution. These effects can be considered via the axial dispersion reactor model, where a diffusion coefficient was used to describe the total contribution of these non-ideal factors.[26–28] However, the application of this model is still limited, especially the systematic study of the influence of non-ideal flow on the ATRcoP in tubular reactor.

In this work, an axial dispersion reactor model is established to describe the ATRcoP process under different flow patterns in continuous tubular reactor. In addition, the effects of axial dispersion and monomer ratio are considered and various reaction characteristics are analyzed using this reactor model. Finally, to study the advantages and disadvantages of plug flow and complete mixing flow, the same ATRcoP process in single CSTR is simulated and the simulation results are compared with those in tubular reactor.

2.. Model Development

2.1.. ATRcoP Mechanism and Kinetic Equations

The reaction mechanism of ATRcoP was simplified in order to facilitate the consequent calculation. All the reasonable assumptions used herein are shown as follows:[29–35]

1. The activity of living chains and dormant chains is only dependent on their terminal unit;
2. All the intrinsic rate coefficients used in this work are not relevant to chain length, which means that they are all constants;
3. Chain transfer reaction only includes the transfer from living chain to monomer;
4. Termination reaction includes the combination and disproportionation termination;
5. Other side reactions like thermal initiation and β-H elimination are ignored.

Based on the above assumptions, the elementary reactions of ATRcoP and the kinetic equations of different ATRcoP components can be obtained, which are shown in Table 1 and 2, respectively.

Table 1. Elementary reactions of ATRcoP.

Reactions
Initiation
$RX + C \xrightarrow{k_a} R^{\bullet} + \mathrm{CX}$
$R^{\bullet} + \mathrm{CX} \xrightarrow{k_{da}} RX + C$
$R^{\bullet} + M_i \xrightarrow{k_{in,i}} RM^{\bullet}_{i,1}$
Propagation
$RM_{i,r}X + C \xrightarrow{k_{a,i}} RM^{\bullet}_{i,r} + \mathrm{CX}$
$RM^{\bullet}_{i,r} + \mathrm{CX} \xrightarrow{k_{da,i}} RM_{i,r}X + C$
$RM^{\bullet}_{i,r} + M_j \xrightarrow{k_{p,ij}} RM^{\bullet}_{j,r+1}$
Transfer
$RM^{\bullet}_{i,r} + M_j \xrightarrow{k_{tr,ij}} RM_{i,r} + M^{\bullet}_j$
Termination
$RM^{\bullet}_{i,r} + RM^{\bullet}_{j,s} \xrightarrow{k_{tc,ij}} RM_{r+s}R$
$RM^{\bullet}_{i,r} + RM^{\bullet}_{j,s} \xrightarrow{k_{td,ij}} RM_{i,r} + RM_{j,s}$

Macromol. React. Eng. 2015, DOI: 10.1002/mren.201400056

Table 2. Kinetic equations of different ATRcoP components.

Equations
Initiator $r_{RX} = -k_a[RX][C] + k_{da}[R^\bullet][CX]$
Activator $r_C = k_{da}[R^\bullet][CX] - k_a[RX][C] + \sum_i \sum_{r=1}^{\infty} k_{da,i}[RM_{i,r}^\bullet][CX] - \sum_i \sum_{r=1}^{\infty} k_{a,i}[RM_{i,r}X][C]$
Deactivator $r_{CX} = -k_{da}[R^\bullet][CX] + k_a[RX][C] - \sum_i \sum_{r=1}^{\infty} k_{da,i}[RM_{i,r}^\bullet][CX] + \sum_i \sum_{r=1}^{\infty} k_{a,i}[RM_{i,r}X][C]$
Primary radical $r_{R^\bullet} = -\sum_i k_{in,i}[M_i][R^\bullet] - k_{da}[R^\bullet][CX] + k_a[RX][C]$
Monomer $r_{M_i} = -k_{in,i}[R^\bullet][M_i] - \sum_j \sum_{r=1}^{\infty} k_{p,ji}[RM_{j,r}^\bullet][M_i]$
Living chain $r_{RM_{i,r}^\bullet} = \sum_j k_{p,ji}[RM_{j,r-1}^\bullet][M_i] - \sum_j k_{p,ij}[RM_{i,r}^\bullet][M_j] + k_{a,i}[RM_{i,r}X][C] - k_{da,i}[RM_{i,r}^\bullet][CX] - \sum_j \sum_{s=0}^{\infty} k_{t,ij}[RM_{i,r}^\bullet][RM_{j,s}^\bullet] - \sum_j k_{tr,ij}[RM_{i,r}^\bullet][M_j]$
Dormant chain $r_{RM_{i,r}X} = k_{da,i}[RM_{i,r}^\bullet][CX] - k_{a,i}[RM_{i,r}X][C]$
Dead chain formed by coupling termination $r_{RM,R} = \frac{1}{2} \sum_i \sum_j \sum_{s=0}^{r} k_{tc,ij}[RM_{i,s}^\bullet][RM_{j,r-s}^\bullet]$
Dead chain formed by disproportionation termination and chain transfer $r_{RM_r} = \sum_i \sum_j \sum_{s=0}^{\infty} k_{td,ij}[RM_{i,r}^\bullet][RM_{j,s}^\bullet] + \sum_i \sum_j k_{tr,ij}[RM_{i,r}^\bullet][M_j]$

2.2.. Method of Moments

By using the method of moments,[36–38] the sets of kinetic equations are converted into moment equations, which can be solved conveniently. The definitions of moments depend on the four different kinds of macromolecules in ATRcoP system, namely living chains, dormant chains, dead chains formed by combination termination, and dead chains formed by disproportionation termination, and chain transfer. Four different moments are defined and shown in **Table S1**. The corresponding moment equations are listed in **Table S2**.

In addition, the reaction characteristics of ATRcoP can be expressed by moments, such as number-average molecular weight (M_n), weight-average molecular weight M_w, dispersity ($Đ$), instantaneous copolymer composition (F_A or F_B), and chain-end functionality (F_t). The moment expressions of these characteristics are shown in Table 3.

2.3.. Reactor Model

A mathematical model of tubular reactor for ATRcoP is developed. In an actual tubular reactor, the flow pattern of

Table 3. Moment expressions of characteristics of ATRcoP.

Characteristics	Moment expressions
Number-average molecular weight	$M_n = \frac{\sum_i (\mu_i^1+\lambda_i^1)+\phi^1+\psi^1}{\sum_i (\mu_i^0+\lambda_i^0)+\phi^0+\psi^0} \cdot \sum_i \frac{X_i n_i W_i}{\sum_j (X_i n_i)}$
Weight-average molecular weight	$M_w = \frac{\sum_i (\mu_i^2+\lambda_i^2)+\phi^2+\psi^2}{\sum_i (\mu_i^1+\lambda_i^1)+\phi^1+\psi^1} \cdot \sum_i \frac{X_i n_i W_i}{\sum_j (X_i n_i)}$
Dispersity	$Đ = \frac{M_w}{M_n}$
Instantaneous copolymer composition	$F_i = \frac{k_{in,i}[R\cdot][M_i]+\sum_j k_{p,ji}\mu_o^j[M_i]}{\sum_i k_{in,i}[R\cdot][M_i]+\sum_i\sum_j k_{p,ji}\mu_0^j[M_i]}$
Chain-end functionality	$F_t = \frac{\sum_i \lambda_i^0}{\sum_i \mu_i^0+\sum_i \lambda_i^0+\psi^0+\phi^0}$

reactants is far more complex than the ideal plug flow because of existence of molecule diffusion, vortex flow and velocity distribution. Accordingly, in the developed reactor model, the total contribution of these three non-ideal factors is described by the axial dispersion.[26–28] The basic descriptions and reasonable assumptions about the model are shown as follows:

1. The radial velocity distribution is assumed to be uniform that in the tubular reactor, and all the particles are flowing to the outlet at the same speed.
2. The radial mixing level of reaction mass is excellent that there exists no concentration or temperature field in radial direction.
3. The non-ideal diffusion movements formed by molecule diffusion, vortex flow, and velocity distribution are only exist in axial direction and are described using a diffusion coefficient (D_a) by Fick's Law.
4. The value of D_a is independent with reaction time t and axial position Z. It only depends on reactor structure, operating conditions and flow pattern of reactants.
5. There exists no short flow or dead zone volume in tubular reactor.
6. The temperature of reaction mass during the whole process of ATRcoP is assumed to be constant.

Herein, Figure 1 shows the axial dispersion exists in tubular reactor. Based on above assumptions, the mass balance equation for Component I in the infinitesimal volume (dV_r) can be expressed as follows:

$$uA_r c_I + D_a A_r \frac{\partial}{\partial Z}(c_I + \frac{\partial c_I}{\partial Z} dZ) = uA_r(c_I + \frac{\partial c_I}{\partial Z} dZ) + D_a A_r \frac{\partial c_I}{\partial Z} + \frac{\partial c_I}{\partial t} A_r dZ - r_I dV_r \quad (1)$$

i.e.,

$$\frac{\partial c_I}{\partial t} = D_a \frac{\partial^2 c_I}{\partial Z^2} - u\frac{\partial c_I}{\partial Z} + r_I \quad (2)$$

where u, A_r, c_I, Z, and r_I represent axial velocity of reaction mass, cross-sectional area of tubular reactor, concentration of component I, axial position in tubular reactor, and intrinsic reaction rate of component I, respectively.

At the inlet of tubular reactor, the Danckwerts boundary condition is accepted and shown as follows:

$$c_I|_{Z=0} = c_I|_{Inlet} + \frac{D_a}{u}\frac{dc_I}{dZ}|_{Z=0} \quad (3)$$

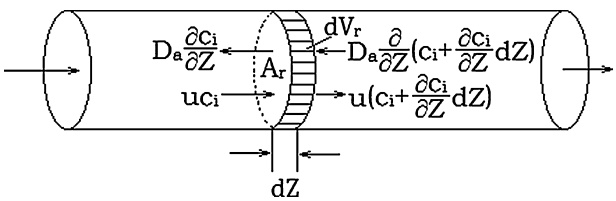

Figure 1. The axial dispersion model in tubular reactor.

Macromol. React. Eng. 2015, DOI: 10.1002/mren.201400056

At the outlet of tubular reactor, the gradient in concentration is set to be zero:

$$\frac{dc_I}{dZ}|_{Z=Z} = 0 \tag{4}$$

The value of D_a is difficult to be obtained, so the Peclet number (*Pe*) is introduced that can be conveniently ensured by fitting the experimental data. The definition of *Pe* is the ratio of convection to diffusion:

$$Pe = \frac{Zu}{D_a} \tag{5}$$

When increasing the value of *Pe*, the flow pattern of reaction mass becomes more approximate to ideal plug flow; otherwise it tends to be complete mixing flow. The installation of internal components in tubular reactor can improve the mixing level of reaction mass, thus decreasing the *Pe* value.

With the definition of *Pe*, Equation (2) can be rewritten as follow:

$$\frac{\partial c_I}{\partial t} = \frac{Zu}{Pe} \cdot \frac{\partial^2 c_I}{\partial Z^2} - u\frac{\partial c_I}{\partial Z} + r_I \tag{6}$$

It can be seen from Equation (6) that concentration of Component I has a function of two variables, i.e., reaction time and axial position. Both of them should be considered during the simulation. For example, the evolution of total monomer conversion X_{Total} with reaction time and axial position are different, which are shown in Equation (7) and (8), respectively:

$$X_{Total}|_Z = \frac{[M_A]|_{Z=0} + [M_B]|_{Z=0} - ([M_A]|_Z + [M_B]|_Z)}{[M_A]|_{Z=0} + [M_B]|_{Z=0}} \tag{7}$$

$$X_{Total}|_t = \frac{[M_A]|_{t=0} + [M_B]|_{t=0} - ([M_A]|_t + [M_B]|_t)}{[M_A]|_{t=0} + [M_B]|_{t=0}} \tag{8}$$

2.4.. Model Implementation

The kinetic parameters are directly obtained from our previous study,[23] which are listed in Table 4. The pdepe-function provided in MATLAB 2012b (8.0) software is used to solve the partial differential equations (mass balance equations for various reaction components).

3.. Results and Discussion

The developed mathematical model for tubular reactor is firstly validated by simulating the ATRP process in the tubular reactor under the same conditions with those in the

Table 4. Kinetic parameters for ATRcoP of MMA and HEMA-TMS in Simulation.

Kinetic Parameters	Values	Refs.
$k_{in,A}$,$k_{p,AA}$ (L/mol · s)	$10^{6.427}\exp[-22360/(RT)]$	[39]
$k_{in,B}$,$k_{p,BB}$ (L/mol · s)	$10^{6.954}\exp[-21900/(RT)]$	[40]
$k_{tc,AA}$ (L/mol · s)	1.0×10^7	[41]
$k_{td,AA}$ (L/mol · s)	$k_{tc,AA} \times 2.57 \times 10^3\exp[-17113/(RT)]$	[41]
$k_{tc,BB}$ (L/mol · s)	0.99×10^6	[42]
$k_{td,BB}$ (L/mol · s)	1.1×10^5	[42]
r_A	0.86	[43]
r_B	0.66	[43]
$k_{tr,AA}$ (1/s)	0.0198	[29]
$k_{tr,BB}$ (1/s)	0.0122	[29]
$k_{t,AB}$,$k_{t,BA}$ (L/mol · s)	$(k_{t,AA} \times k_{t,BB})^{1/2}$	[44]
$k_{tr,AB}$,$k_{tr,BA}$ (1/s)	$(k_{tr,AA} \times k_{tr,BB})^{1/2}$	Use the method in [44]
$k_{tc,AB}$,$k_{tc,BA}$ (L/mol · s)	$(k_{tc,AA} \times k_{tc,BB})^{1/2}$	Use the method in [44]
$k_{td,AB}$,$k_{td,BA}$ (L/mol · s)	$(k_{td,AA} \times k_{td,BB})^{1/2}$	Use the method in [44]
$k_{t,AA}$ (L/mol · s)	$k_{tc,AA} + k_{td,AA} = 9.9 \times 10^7$	This work
$k_{t,BB}$ (L/mol · s)	$k_{tc,BB} + k_{td,BB} = 1.1 \times 10^6$	This work
k_a (L/mol · s)	$(k_{a,A} + k_{a,B})/2$	This work
k_{da} (L/mol · s)	$(k_{da,A} + k_{da,B})/2$	This work
$k_{a,A}$ (L/mol · s)	1.2853	This work
$k_{a,B}$ (L/mol · s)	1.2051	This work
$k_{da,A}$ (L/mol · s)	1.2597×10^6	This work
$k_{da,B}$ (L/mol · s)	1.2216×10^7	This work

open report.[19] Then the ATRcoP processes of MMA and HEMA-TMS in tubular reactor are simulated and reaction behaviors under different levels of axial dispersion are obtained. Finally, to analyze the difference of copolymer properties between CSTR and PFR, the same ATRcoP process in these two different reactor models are simulated. The CSTR model used in this work comes from our previous research work.[23] Besides, the *Pe* in tubular reactor model is set to a certain value to make sure that the axial dispersion in the tube is negligible and the flow pattern of reactants approaches to PFR.

3.1.. Model Validation

The experimental data of ATRP of MMA from Shen et al.[19] were used to validate the obtained mathematical model. In the experiment, the catalyst complex is supported by silica gel in tubular reactor. Because of the limitation of reactor model, the silica-supported ATRP catalyst system is replaced by an ideal model. In the simulation, the catalyst complex is dissolved in solvent and there is no inputting and outputting during the reaction. In addition, the catalyst complex is evenly distributed in reactor, namely, there does not exist concentration field. Furthermore, the loss of catalyst complex by flow of reactants is neglected, and there is no trapping of polymer chains in the silica gel. Based on above assumptions, the mass balance equation for C (CuBr) and CX ($CuBr_2$) in the reactor can be expressed as follows:

$$\frac{\partial[C]}{\partial t} = r_C \tag{9}$$

$$\frac{\partial[CX]}{\partial t} = r_{CX} \tag{10}$$

When the *Pe* value is set to be 50, good agreement between the simulation results and experimental data is obtained, showing that the level of axial dispersion is really limited during the experiment. The fitting results are shown in Figure 2. Figure 2(a) shows the development of MMA conversion at reactor outlet versus polymerization time. Note that, the MMA conversion begins to decrease after 70 h, the main cause of this phenomenon is that the activator CuBr used in the tubular reactor is supported by silica gel. The total amount of CuBr is limited and it tends to taper off during the polymerization because of the continuous conversion from CuBr to $CuBr_2$. When the amount of CuBr decreases to a certain level, the formation of living chains and the consumption of monomer is significantly reduced, and these changes ultimately result in the decline of monomer conversion. Figure 2(b) shows the molecular weight and dispersity of polymers at reactor outlet versus time. The *Đ* value of PMMA is about 1.8, which is a little higher than the experimental result. The reason may be the formation of dead chains by trapping the polymer chains into the silica gel, which is not included in the model. In addition, the effect of backmixing on dispersity may be non-ignorable. As a whole, Figure 2 shows a good agreement between experiment and simulation. Therefore, the obtained mathematical model can be used for further studies on reaction characteristics of ATRcoP in tubular reactor.

3.2.. Model Application in Tubular Reactor

The ATRcoP of MMA and HEMA-TMS in a tubular reactor with a length of 3 m and a internal diameter of 0.01 m is simulated. The catalyst complex is added into the reactor before the reaction and there is no inputting and

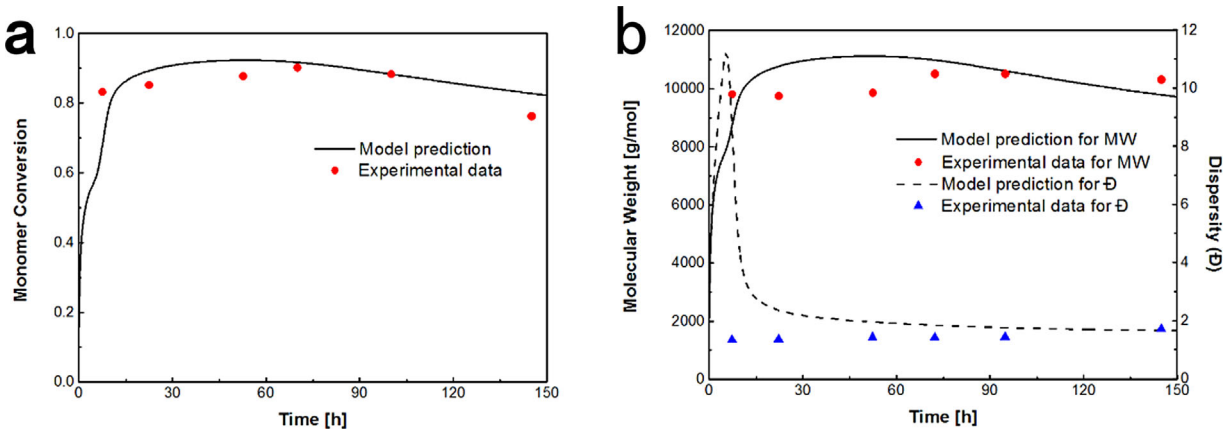

Figure 2. Comparison of the simulated results and experimental data of ATRP of MMA in tubular reactor under the same conditions that used in ref 19: (A) The monomer conversion at reactor outlet vs time; (B) The molecular weight and dispersity at reactor outlet versus time. [The rate coefficients used in this case are listed in Table 4, except that the values of k_a and k_{da} are set to be 5.0 and 6.0 $\times$ 10^5 L mol s^{-1}, respectively, due to the different activities of 1,1,4,7,10,10-Hexamethyltriethylenetetramine (HMTETA) and 4,4′-Dinonyl-2,2′-bipyridyl (dNbpy)].

Macromolecular Journals
Macromol. React. Eng. **2015,** DOI: 10.1002/mren.201400056

Table 5. Simulation conditions for ATRcoP in tubular reactor.

No.	Q_i(L/s)	Pe	Composition in feeding flow and initial charge (mol/L)*				
			$[M_A]$	$[M_B]$	[RX]	[C]	[CX]
1	3×10^{-6}	0.5	1	1	0.01	0.01	5×10^{-4}
2	3×10^{-6}	5	1	1	0.01	0.01	5×10^{-4}
3	3×10^{-6}	50	1	1	0.01	0.01	5×10^{-4}
4	3×10^{-6}	500	1	1	0.01	0.01	5×10^{-4}
5	3×10^{-6}	50	0.5	1.5	0.01	0.01	5×10^{-4}
6	3×10^{-6}	50	1.5	0.5	0.01	0.01	5×10^{-4}

outputting. The feeding rates of initiator and monomer are set to be 3×10^{-6} L/s. The other specific simulation conditions are shown in Table 5. To describe the actual flow pattern of reactants in tubular, the simulation results of four different values of *Pe* are shown as follows.

Figure 3 shows the development of total monomer conversion X_{Total} along the tube after 40 h. When $Pe = 0.5$, the X_{Total} at inlet of reactor is as high as 58%, which is impossible for newly added monomers. The only explanation is that there exists significant axial dispersion and high degree of backmixing in tubular reactor. Because of the axial dispersion against the convection direction, the X_{Total} increases slowly along the tube and finally reaches 68% at reactor outlet.

When the value of *Pe* increases, the flow pattern of reaction mass tends to be plug flow and the degree of backmixing becomes smaller. When $Pe = 50$, X_{Total} increases from 5% at inlet to 90% at outlet, showing that the gradient in conversion is quite significant along the tube. When *Pe* increases to 500, the obtained curve is almost the same with that for $Pe = 50$, indicating the degree of backmixing is low enough and the flow pattern is almost the ideal plug flow when $Pe = 50$. In conclusion, the suitable value of *Pe* for plug flow in this model is around 50.

Figure 4 shows the evolution of X_{Total} at reactor outlet with respect to time. When reaction time increases to 40 h, the X_{Total} for $Pe = 0.5$, 5, 50, and 500 are 72%, 83%, 90%, and 91%, respectively. The plug flow pattern with lowest degree of axial dispersion has the highest level of monomer consumption. Meanwhile, all the curves are found to be downward and X_{Total} begins to decline later for higher value of *Pe*. The main cause of these phenomenons may be the variation of concentrations of CuBr and $CuBr_2$ during the copolymerization process.

For the ATR(co)P system in tubular reactor, there is no inputting or outputting of CuBr and $CuBr_2$, and they can transform into each other by the ATR(co)P equilibrium. The formation of living chains is accompanied with the consumption of activator and the generation of deactivator. Figure 5 shows the development of concentration of CuBr and $CuBr_2$ versus time. In the flow with high value of *Pe*, with the continuous conversion of CuBr to $CuBr_2$, the

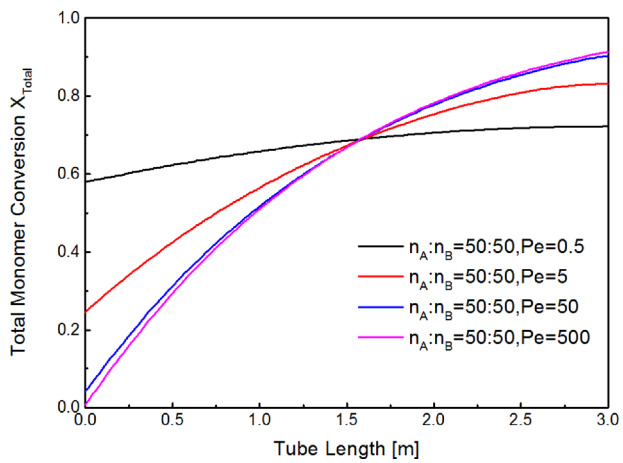

Figure 3. The simulated total monomer conversion versus the tube length after 40 h for the ATRcoP in the tubular reactor.

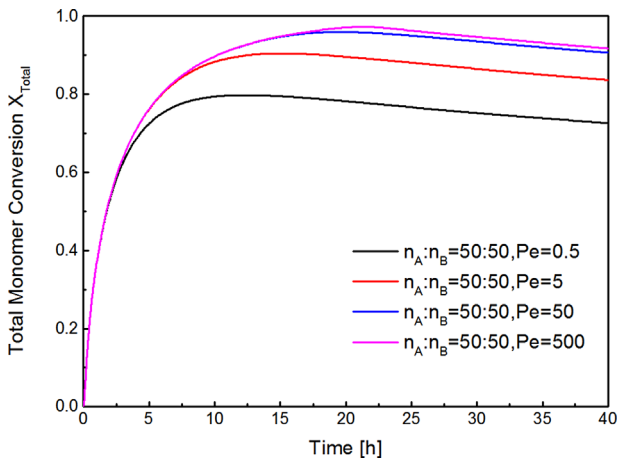

Figure 4. The simulated total monomer conversion at reactor outlet versus the time for the ATRcoP in the tubular reactor.

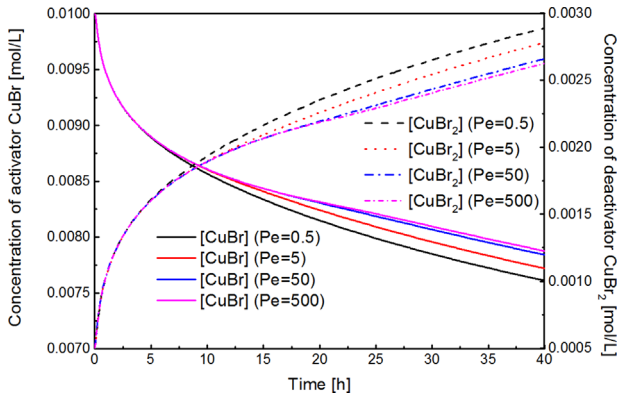

Figure 5. The simulated activator and deactivator concentrations versus the time for the ATRcoP in the tubular reactor.

activation rate R_{act} proceeds more slowly and the concentration of living chains decreases, so the consumption of monomer reduces over a period of time. The concentration of living chains versus time for different Pe values is shown in Figure S1. In the flow with low *Pe* value, the effect of axial dispersion is significant. At the beginning of copolymerization with higher concentration of dormant chains due to backmixing, the ATR(co)P equilibrium is prefer to convert more CuBr to $CuBr_2$ and generate more living chains, which promotes the termination reaction. Thus, the more dead chains are produced and consumption of monomer slows down earlier than that in flow with low level of axial dispersion. The lower the *Pe* value is, the higher the level of axial dispersion is, so that the declination of CuBr concentration becomes more significant.

Figure 6 shows the dispersity of copolymers along the tube after 40 h. For $Pe = 0.5$, the $Đ$ value is between 1.86 and 2.08 because of severe axial dispersion. For $Pe = 5$, the flow pattern in tubular reactor is a form somewhere between plug flow and completely mixed flow, so the dispersity of copolymers narrows down slightly that the $Đ$ value is around 1.4. For $Pe = 50$ and 500, the reactant moves in the form of plug flow and the $Đ$ value is lower than 1.1. Figure 7 shows that the dispersity of copolymers at reactor outlet increases gradually with time for $Pe = 0.5$ and 5, but when $Pe = 50$ and 500, there exists an obvious decline of $Đ$ value after 22 h. As stated previously, the consumption of activator in reaction process results in the decline of the concentration of living chain and the reduction of termination reaction. Thus the dispersity of copolymers narrows down under low backmixing condition. When there exists the obvious axial dispersion, the effect of backmixing surpasses the effect of consumption of activator and the formation of dead chains is promoted, therefore the dispersity of copolymers becomes broader.

It can be seen from Figure 8 that for each value of *Pe*, the number-average molecular weight increases linearly with X_{Total}. Although the nonlinear part at the very beginning of copolymerization is observed, it can still conclude that the copolymerization process is reversible-deactivation radical polymerization. Furthermore, the final value of molecular weight is found to be proportional to *Pe*, that is to say, the average chain length of copolymers in plug flow is longer than that in tube with significant axial dispersion.

Figure 9 shows the evolution of instantaneous MMA composition F_A along the copolymer chain for different monomer ratios and *Pe* values. For different values of *Pe* with the constant monomer ratio (50:50), there is almost no effect of *Pe* on copolymer composition because the obtained curves of F_A are overlapped. When under the constant value of *Pe* (50), the variation ranges of F_A are 12–29%, 46–52%, and 71–76% for $[M_A]/([M_A]+[M_B]) = 25$, 50, and 75%,

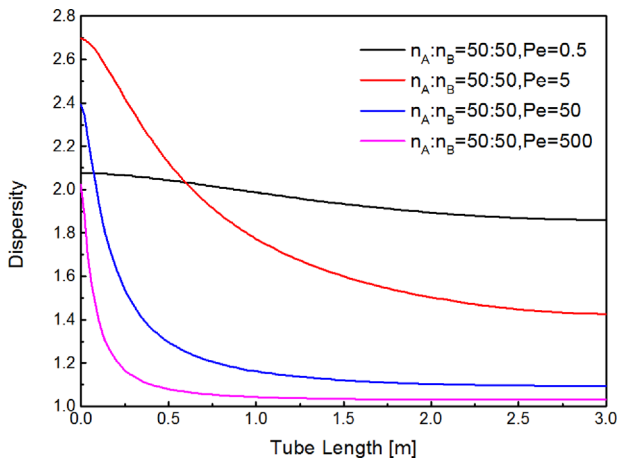

Figure 6. The simulated copolymer dispersity versus the tube length after 40 h for the ATRcoP in the tubular reactor.

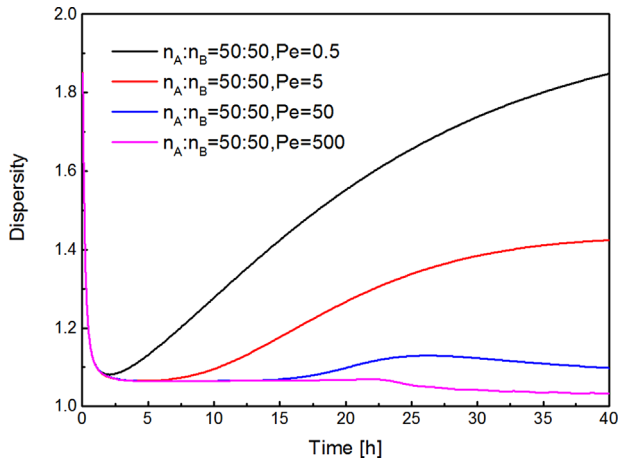

Figure 7. The simulated copolymer dispersity at reactor outlet versus the time for the ATRcoP in the tubular reactor.

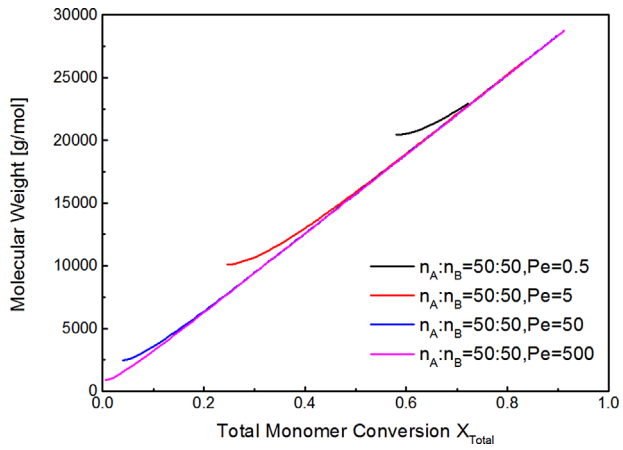

Figure 8. The simulated copolymer molecular weight versus the total monomer conversion after 40 h for the ATRcoP in the tubular reactor.

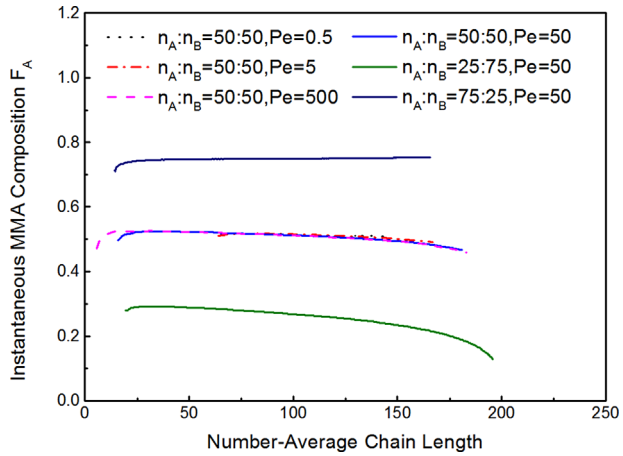

Figure 9. The simulated instantaneous MMA composition versus the copolymer number-average chain length for the ATRcoP in the tubular reactor.

respectively, showing that F_A and the proportion of MMA in feeding flow are in good agreement. The obtained results are in accordance with those shown in some other work.[45,46] The composition of spontaneous copolymers produced by tubular reactor is mainly influenced by the reactivity ratios of two kinds of monomers.[47] Because of the similar reactivity between MMA and HEMA-TMS (0.86 and 0.66), the gradient in copolymer composition is found to be not obvious for each case.

Figure 10 shows the development of end-group functionality F_t versus X_{Total}. At the end of reaction, The F_t values are about 90% in all cases. In addition, the highest level of F_t is obtained when $Pe = 500$, meaning that the termination reaction is the slowest. The result verifies the previous analysis about the influence of flow pattern on termination reaction.

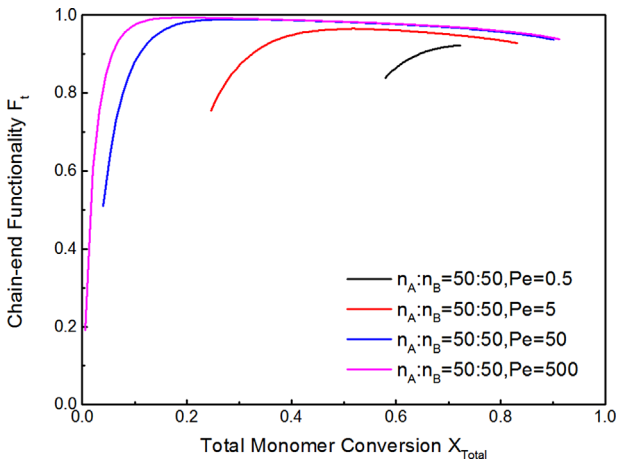

Figure 10. The simulated chain-end functionality versus the total monomer conversion for the ATRcoP in the tubular reactor.

3.3.. Comparison in CSTR and PFR

Generally, the completely mixed flow and ideal plug flow can be realized in a CSTR and a tubular reactor, respectively. The studies of ATRcoP in these two extreme conditions are of great importance for industrialization of reversible-deactivation radical polymerization.

The reaction characteristics of ATRcoP in these two reactors are simulated. The tubular reactor model and the design of tube remain the same with those in section 3.2. To ensure that the flow pattern in the tube is close to plug flow, the *Pe* values are set to be 50 and 500. The CSTR model used in previous work[23] is adopted in this work. For comparison, the feeding rate and reaction volume of CSTR are the same with those of tubular reactor. The detailed simulation conditions are shown in Table 6.

As shown in Figure 11, the final values of X_{Total} in CSTR and PFR are 78 and 90%, respectively. In the same feeding rate and reaction volume, the monomer conversion in tubular reactor is found to be higher than that in CSTR. The main cause of this phenomenon is that the maximum level of backmixing in CSTR has the negative influence on the monomer conversion. In addition, the monomer conversion in CSTR is inversely correlated with the feeding flow rate. By increasing the feeding rate, the mean residence time is shortened, so the monomer conversion declines. In tubular reactor, the monomer conversion is mainly influenced by the flow pattern of reactant. For ideal plug flow in tubular reactor, the variation of monomer conversion along the tube is similar with the evolution of monomer conversion versus time in bath reactor. For plug flow with significant axial dispersion, the tubular reactor can be considered as a CSTR.

In CSTR, because of the residence time distribution resulting from the backmixing, the dispersity of copolymers is much broader than that in other reactors. For tubular

Table 6. Simulation conditions for ATRcoP in CSTR and Tubular Reactor.

Reactor	Q_i(L/s)	Pe	Composition in feeding flow and initial charge (mol/L)*					V(L)
			$[M_A]$	$[M_B]$	[RX]	[C]	[CX]	
CSTR	3×10^{-6}	—	1	1	0.01	0.01	5×10^{-4}	0.2355
CSTR	3×10^{-6}	—	0.5	1.5	0.01	0.01	5×10^{-4}	0.2355
CSTR	3×10^{-6}	—	1.5	0.5	0.01	0.01	5×10^{-4}	0.2355
PFR	3×10^{-6}	50	1	1	0.01	0.01	5×10^{-4}	0.2355
PFR	3×10^{-6}	500	1	1	0.01	0.01	5×10^{-4}	0.2355
PFR	3×10^{-6}	500	0.5	1.5	0.01	0.01	5×10^{-4}	0.2355
PFR	3×10^{-6}	500	1.5	0.5	0.01	0.01	5×10^{-4}	0.2355

*All the abbreviations are the same as those in Table 5.

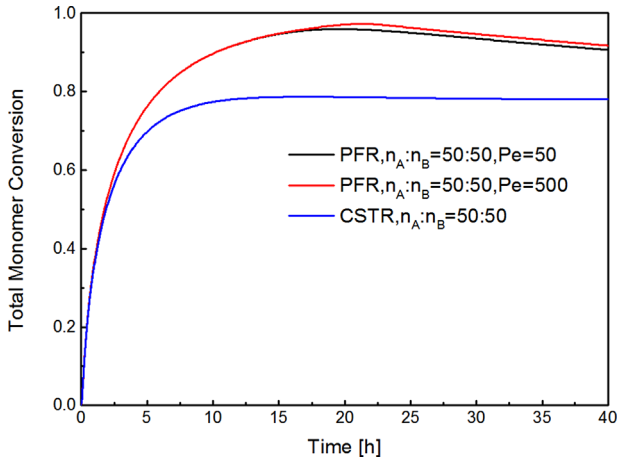

Figure 11. The simulation results for the ATRcoP processes in CSTR and PFR: the total monomer conversion at reactor outlet versus the time.

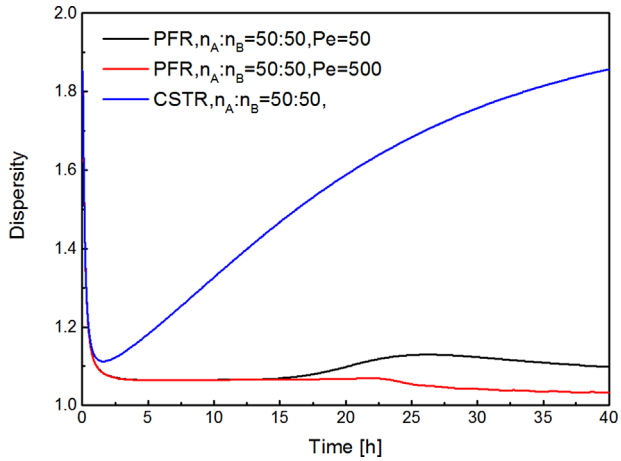

Figure 12. The simulation results for the ATRcoP processes in CSTR and PFR: the copolymer dispersity at reactor outlet versus the time.

reactor, as before, when the flow pattern of reactants is close to plug flow, the dispersity of copolymers becomes much narrower than that in CSTR. As shown in Figure 12, with the processing of copolymerization, the $Đ$ value in CSTR increases rapidly, whereas in tubular reactor for $Pe = 50$ and 500 it remains in a low level.

The curves of F_A along the copolymer chain produced in complete mixing flow and plug flow are shown in Figure 13. With the same monomer molar ratio, the evolutions of F_A in two different reactors are almost the same, meaning that the copolymer composition is irrelevant to flow pattern. In addition, the gradient in composition of synthetic copolymers is not obvious that the variation range of F_A along the chain is highly consistent with the initial monomer molar ratio. The copolymers produced in CSTR and tubular are spontaneous and their compositions only depend on the reactivity ratios of monomers. Because of the similar

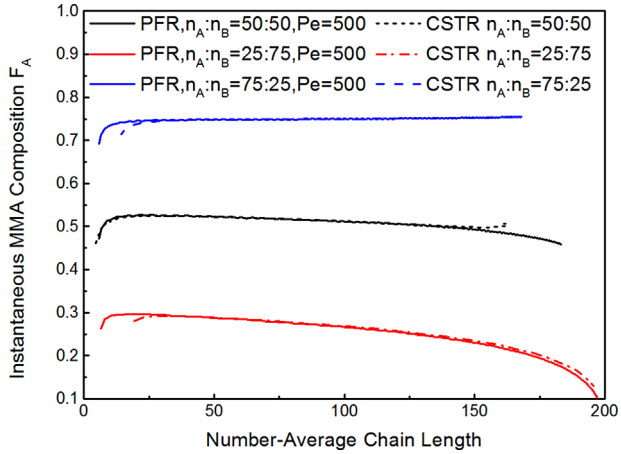

Figure 13. The simulation results for the ATRcoP processes in CSTR and PFR: the instantaneous MMA composition versus the number-average chain length.

Macromolecular Journals
Macromol. React. Eng. **2015,** DOI: 10.1002/mren.201400056

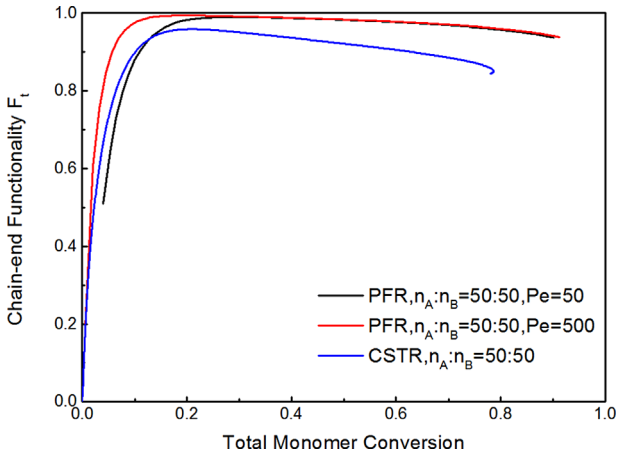

Figure 14. The simulation results for the ATRcoP processes in CSTR and PFR: the chain-end functionality versus the total monomer conversion.

reactivity ratio of MMA and HEMA-TMS in this work, the composition along the copolymer chain is inconspicuous.

As can be seen from the Figure 14, the chain-end functionality of copolymers produced in tubular reactor under the condition of plug flow is still higher than 90% at the end of reaction. However, the declination of F_t in CSTR is more rapid and obvious than that in plug flow. Similar to the plug flow with significant axial dispersion in tubular reactor, the backmixing of reactants in CSTR causes the acceleration of termination reaction, and thus the declination of chain-end functionality.

4.. Conclusion

To study the influence of flow pattern on reaction characteristics of copolymerization in tubular reactor, the plug flow reactor model used in this work is coupled with axial dispersion model. Before the formal simulation, the developed mathematical model is firstly verified by fitting experimental data from research work of Shen et al. with the simulation results from this model under the same condition. The fitting result is in good agreement with experimental data, meaning that the developed mathematical model can be used for further study of ATRcoP process in tubular reactor.

It can be concluded from simulation results that the influence of flow pattern in tubular reactor on properties of copolymers is significant. For plug flow pattern, the final copolymers are found to be long chain length, narrow dispersity and high F_t. The existence of axial dispersion results in the declination of monomer conversion, broadening of dispersity and decreasing of F_t. Besides, the curves of F_A along the chain for different values of Pe are overlapped, indicating that the copolymer composition has less relationship to flow pattern of reactants.

Under the same feeding rate and reaction volume, the plug flow in tubular reactor has some advantages over the complete mixing flow in CSTR, including higher monomer conversion, narrower dispersity and better chain-end functionality. However, the compositions of copolymers in these two reactors are very similar, indicating that the flow pattern has little influence on copolymer composition.

In conclusion, this research work shows the various reaction characteristics of ATRcoP process in tubular reactor by simulation, which has important implications for applied research of reversible-deactivation radical polymerization in actual production.

5.. Nomenclature

A_r	cross-sectional area of tubular reactor (m^2)
C_I	concentration of the species I in the reactor (mol L^{-1})
C	activator or catalyst at the lower oxidation state
CX	deactivator or catalyst at the higher oxidation state
K_{eq}	equilibrium coefficient of the activation/deactivation reaction
k_a	activation rate constant for initiator ($L(mol\,s)^{-1}$)
$k_{a,i}$	activation rate constant for dormant chains with the i-type of terminal unit ($L(mol\,s)^{-1}$)
k_{da}	deactivation rate constant for primary radical ($L(mol\,s)^{-1}$)
$k_{da,i}$	deactivation rate constant for living chains with i-type of terminal unit ($L\,(mol\,s)^{-1}$)
$k_{in,I}$	initiation rate constant for monomer i adding to primary radical ($L\,(mol\,s)^{-1}$)
$k_{p,ij}$	chain propagation rate constant for monomer j adding to living chains with the i-type of terminal unit ($L\,(mol\,s)^{-1}$)
$k_{tr,ij}$	chain transfer rate constant for monomer j adding to living chains with the i-type of terminal unit ($L\,(mol\,s)^{-1}$)
$k_{tc,ij}$	coupling termination rate constant between living chains with i and j types of terminal unit ($L\,(mol\,s)^{-1}$)
$k_{td,ij}$	disproportional termination rate constant between living chains with i and j types of terminal unit ($L\,(mol\,s)^{-1}$)
$k_{t,ij}$	termination rate constant between living chains with i and j types of terminal unit ($L\,(mol\,s)^{-1}$)
M_i	monomer i
M_n	number-average molecular weight
M_w	weight-average molecular weight
n_i	mole number of monomer i (mol)
Q_i	volume flow rate of inlet or outlet, L/s
$R^\bullet$	primary radical
RX	initiator

$RM_{i,r}X$ dormant chain with length r and i-type of unit adjacent to halogen atom
$RM_{i,r}$ dead chains with length r formed by disproportionation termination or chain transfer to monomer
RM_rR dead chains with length r formed by coupling termination
$RM_{i,r}$ propagating radical chain with length r and i-type of terminal unit
r_I intrinsic reaction rate of the component I, mol m^3 s
r_A reactivity ratio of monomer A
r_B reactivity ratio of monomer B
r_n number-average chain length
r_w weight-average chain length
u axial velocity of reaction mass ($m\,s^{-1}$)
W_i conversion of monomer i
X_i monomer molecular weight of monomer i (g mol^{-1})
X_{Total} total monomer conversion
Z axial position in tubular reactor, m

6.. Greek Letters

λ_i^m mth-order moment of dormant chains with the i-type of terminal unit
μ_i^m mth-order moment of living chains with the i-type of terminal unit
ϕ^m mth-order moment of dead chains formed by coupling termination
ϕ^m mth-order moment of dead chains formed by disproportionation termination or chain transfer to monomer
[] molar concentration ($mol\,L^{-1}$)

7.. Subscripts

A MMA
B HEMA-TMS

Acknowledgments: The authors thank the National Natural Science Foundation of China (No. 21276213, U146210010), the Research Fund for the Doctoral Program of Higher Education (No. 20130073110077), the National High Technology Research and Development Program of China (No. 2013AA032302), and the State-Key Laboratory of Chemical Engineering of Tsinghua University (No. SKL-ChE-13A05) for supporting this work.

Received: November 18, 2014; Revised: January 25, 2015; Published online: January 01, 2015; DOI: 10.1002/mren.201400056

Keywords: ATRP; flow mode; kinetic model; method of moments; polymerization behavior

[1] W. A. Braunecker, K. Matyjaszewski, *Prog. Polym. Sci.* **2007**, *32*, 93.
[2] N. Chan, J. Meuldijk, M. F. Cunningham, R. A. Hutchinson, *Ind. Eng. Chem. Res.* **2013**, *52*, 1.
[3] D. Parida, C. A. Serra, D. K. Garg, Y. Hoarau, R. Muller, M. Bouquey, *Macromol. React. Eng.* **2014**, *8*, 597.
[4] T. Yoshida, A. Tsunoda, H. Koide, T. Hoshina, *J. Chem. Eng. Jpn.* **1997**, *30*, 677.
[5] A. Bahadori, *J. Disper. Sci. Technol.* **2012**, *33*, 200.
[6] M. Covezzi, G. Mei, *Chem. Eng. Sci.* **2001**, *56*, 4059.
[7] N. Chan, M. F. Cunningham, R. A. Hutchinson, *Polym. Chem.* **2012**, *3*, 1322.
[8] M. Zhang, W. H. Ray, *J. Appl. Polym. Sci.* **2002**, *86*, 1630.
[9] N. Chan, M. F. Cunningham, R. A. Hutchinson, *Polym. Chem.* **2012**, *3*, 486.
[10] N. Chan, M. F. Cunningham, R. A. Hutchinson, *Macromol. React. Eng.* **2010**, *4*, 369.
[11] N. Chan, S. Boutti, M. F. Cunningham, R. A. Hutchinson, *Macromol. React. Eng.* **2009**, *3*, 222.
[12] W. W. Smulders, C. W. Jones, F. J. Schork, *Macromolecules.* **2004**, *37*, 9345.
[13] W. W. Smulders, C. W. Jones, F. J. Schork, *AIChE J.* **2005**, *51*, 1009.
[14] G. Qi, C. W. Jones, J. F. Schork, *Ind. Eng. Chem. Res.* **2006**, *45*, 7084.
[15] J. P. Russum, C. W. Jones, F. J. Schork, *Macromol. Rapid Commun.* **2004**, *25*, 1064.
[16] J. P. Russum, C. W. Jones, F. J. Schork, *nd. Eng. Chem. Res.* **2005**, *44*, 2484.
[17] J. P. Russum, C. W. Jones, F. J. Schork, *AIChE J.* **2006**, *52*, 1566.
[18] S. Zhu, Y. Shen, R. H. Pelton , *US Patent 2,307,438* (**2000**).
[19] Y. Shen, S. Zhu, R. Pelton, *Macromol. Rapid Commun.* **2000**, *21*, 956.
[20] Y. Shen, S. Zhu, *AIChE J.* **2002**, *48*, 2609.
[21] N. Chan, M. F. Cunningham, R. A. Hutchinson, *J. Polym. Sci. Polym. Chem.* **2013**, *51*, 3081.
[22] W. Wang, Y. N. Zhou, L. Shi, Z. H. Luo, *Polym. Eng. Sci.* **2014**, DOI: 10.1002/pen.23972.
[23] W. Wang, Y. N. Zhou, Z. H. Luo, *Ind. Eng. Chem. Res.* **2014**, *53*, 11873.
[24] R. Lemoine-Nava, A. Flores-Tlacuahuac, E. Saldívar-Guerra, *Chem. Eng. Sci.* **2006**, *61*, 370.
[25] T. E. Enright, M. F. Cunningham, B. Keoshkerian, *Macromol. Rapid Commun.* **2005**, *56*, 221.
[26] M. Zhang, W. H. Ray, *J. Appl. Polym. Sci.* **2002**, *86*, 1047.
[27] A. K. Hipp, W. H. Ray, *Chem. Eng. Sci.* **1996**, *51*, 281.
[28] W. J. Yoon, K. Y. Choi, *Polym. Eng. Sci.* **1996**, *36*, 65.
[29] Y. N. Zhou, J. J. Li, Z. H. Luo, *J. Polym. Sci. Part A: Polym. Chem.* **2012**, *50*, 3052.
[30] R. Wang, Y. W. Luo, B. G. Li, S. Zhu, *AIChE J.* **2007**, *53*, 174.
[31] S. P. Zhu, *Macromol. Theory Simul.* **1999**, *8*, 29.
[32] O. Delgadillo-Velazquez, E. Vivaldo-Lima, I. A. Quintero-Ortega, *AIChE J.* **2002**, *48*, 2597.

[33] M. Al-Harthi, J. B. P. Soares, L. C. Simon, *Macromol. React. Eng.* **2007**, *1*, 468.
[34] D. R. D'hooge, M. F. Reyniers, G. B. Marin, *Macromol. React. Eng.* **2009**, *3*, 185.
[35] X. H. Li, W. J. Wang, B. G. Li, S. Zhu, *Macromol. React. Eng.* **2011**, *5*, 467.
[36] P. Pladis, C. Kiparissides, *Chem. Eng. Sci.* **1998**, *33*, 3315.
[37] X. Gao, W. Feng, S. Zhu, H. Sheardown, J. L. Brash, *Macromol. React. Eng.* **2010**, *4*, 235.
[38] L. Bentein, D. R. D'hooge, M-F. Reyniers, G. B. Marin, *Macromol. Theory Simul.* **2010**, *20*, 238.
[39] S. Beuermann, M. Buback, T. P. Davis, R. G. Gilbert, R. A. Hutchinson, O. F. Olaj, J. Russell, G. T. Schweer, A. M. Van Herk, *Macromol. Chem. Phys.* **1997**, *198*, 1545.
[40] M. Buback, C. H. Kurz, *Macromol. Chem. Phys.* **1998**, *199*, 2301.
[41] E. Vivaldo-Lima, R. Garca-Perez, O. J. Celedon-Briones, *Rev. Soc. Quim. Mex.* **2003**, *47*, 22.
[42] M. D. Goodner, H. R. Lee, C. N. Bowman, *Ind. Eng. Chem. Res.* **1997**, *36*, 1247.
[43] D. Brauna, W. K. Czerwinski, F. Tudos, T. Kelenc, B. Turcsanyi, *Die. Angew. Makromol. Chem.* **1990**, *178*, 209.
[44] C. Walling, *J. Am. Chem. Soc.* **1949**, *71*.
[45] A. Szanka, G. Szarka, B. Iván, *Polymer.* **2013**, *54*, 6073.
[46] A. Szanka, G. Szarka, B. Iván, *J. Macromol. Sci., Pure Appl. Chem.* **2014**, *51*, 125.
[47] P. H. M. Van Steenberge, D. R. D'hooge, Y. Wang, M. Zhong, M-F. Reyniers, D. Konkolewicz, K. Matyjaszewski, G. B. Marin, *Macromolecules.* **2012**, *45*, 8519.

Macromol. React. Eng. **2015,** DOI: 10.1002/mren.201400056